

Two Classes of Velocity Regulators for Input-Saturated Motor Drives

Javier Moreno-Valenzuela and Ricardo Campa, *Member, IEEE*

Abstract—This paper deals with the velocity control of motor drives when saturated inputs are considered. Two classes of velocity controllers guaranteeing exponential stability are introduced. The first controller allows nonlinear proportional an integral action, while the other one includes an antiwindup loop. A detailed experimental study is provided, which confirms the theoretical results.

Index Terms—Antiwindup, input saturation, motor drive, proportional–integral (PI) control, velocity control.

NOTATION

Lowercase italic letters stand for scalar variables, e.g., $x \in \mathbb{R}$. Lowercase bold letters stand for vectors, e.g., $\mathbf{x} \in \mathbb{R}^n$. Uppercase italic letters, like A , denote either scalar constants or $n \times n$ matrices. An over dot is used to indicate time differentiation, i.e., $\dot{x} = (d/dt)x$.

I. INTRODUCTION

VELLOCITY regulation and velocity control of electrical motors have many applications in industrial processes and machine tools. The objective of velocity regulation is to maintain the velocity of the motor shaft at a given constant desired reference. In contrast, the goal of velocity control is to accurately track a time-varying desired velocity (see, e.g., [5] and [15] and references therein). Let us notice that the design of stable velocity controllers is important in industrial robots, since they use motor drives provided with an inner velocity feedback loop as the core of the control system [4], [3]. In addition, velocity control has been recognized as an important issue in force control of manipulators [10].

The proportional–integral (PI) control is the most used algorithm to regulate the velocity in motor drives. With a proper tuning, a simple PI controller is enough. However, in order to achieve a desired performance, the physical limitations of the motor should be taken into account. For example, in a real motor drive, the current command is limited to a prescribed maximum value due to the converter protection, magnetic sat-

uration, and motor overheating [2]. As pointed out in the textbook [19, p. 171]: “saturation is probably the most commonly encountered nonlinearity in control engineering.”

In many industrial problems where control engineering is involved, the problem is to achieve output regulation of the system

$$\begin{aligned}\dot{\mathbf{x}}(t) &= A\mathbf{x}(t) + \mathbf{b} \text{sat}(u(t)) \\ y(t) &= \mathbf{c}^T \mathbf{x}(t)\end{aligned}\quad (1)$$

where sat is the standard saturation function, to be defined later, and $u(t)$ is the control input. In other words, the problem is to find a controller $u(t)$, either static or dynamic, such that

$$\lim_{t \rightarrow \infty} [y^* - y(t)] = 0$$

where $y^* \in \mathbb{R}$ is the desired output.

Although that problem was known since 1960s by many control practitioners, papers addressing it in a formal way date from 25 years ago (see, e.g., [8] and references therein). The recent work by Eun *et al.* [6] showed conditions such that the system (1) and (2) can be globally stabilized at $y = y^*$ by designing $u(t)$ through dynamic linear feedback.

To the best of the author’s knowledge, the idea that the signal $u(t)$ in the system (1) and (2) can be designed as a nonlinear function of the state and some dynamic extensions (such as integral actions) required to stabilize the output error $[y^* - y(t)]$ is new. The advantage of the nonlinear feedback is that it can present different slope profiles, e.g., a high slope when the error is small rejects unmodeled dynamics, and a medium or low slope when it is big prevents from large control actions and possible damage of the actuator.

In addition to the problem of stabilization of saturated systems, there is the problem of performance. Actuator saturation can cause windup, i.e., excessive overshoots, long settling times and, in some cases, instability. Particularly, in linear PI controllers, windup consists in the integrator signal drifting to undesirable values so that the integrator produces even larger control signals. For PI controllers, a well-known antiwindup technique is the back-calculation scheme. As pointed out in [13], that method was first described by Fertik and Ross [7] and is mentioned in most introductory literature on the subject, e.g., Åström and Hägglund [1]. However, in the specific case of velocity regulation of linear motor drives, many alternative solutions to avoid integrator windup have been proposed. Shin [20] proposed a PI controller with a conditional antiwindup loop. Essentially, this scheme works by turning off the integral action if saturation is detected. Another conditional approach was proposed by Hodel and Hall [9], which was later revisited

Manuscript received April 2, 2008; revised April 16, 2008, September 10, 2008, November 6, 2008, and December 27, 2008. First published March 16, 2009; current version published June 3, 2009. This work was supported in part by CONACyT, in part by SIP-IPN, and in part by PROMEP, Mexico.

J. Moreno-Valenzuela is with the Centro de Investigación y Desarrollo de Tecnología Digital del Instituto Politécnico Nacional, Tijuana 22510, Mexico (e-mail: moreno@citedi.mx).

R. Campa is with the División de Estudios de Posgrado e Investigación, Instituto Tecnológico de la Laguna, Torreón, Coah 27000, Mexico.

Color versions of one or more of the figures in this paper are available online at <http://ieeexplore.ieee.org>.

Digital Object Identifier 10.1109/TIE.2009.2016515

in [14]. There, the idea was to turn off the integral action if saturation is detected and if the sign of the error signal times the control signal is positive. Recently, analyzing the frequency content of the motor torque command, a method to avoid input saturation which switches between P and PI control modes was introduced in [18]. The work by Jo *et al.* [11] dealt with the problem of magnetic saturation in interior permanent-magnet motors by using an optimal control approach.

Let us point out that the proposal of using a control signal $u(t)$ with a nonlinear PI structure that incorporates some antiwindup strategy to stabilize the output error $[y^* - y(t)]$ of the class of systems (1) and (2) seems to be new.

The main purpose of this paper is to provide solutions to the problem of velocity regulation of motor drives subject to constrained control voltage inputs. First, a framework to design a large class of controllers with a PI structure is proposed. To derive a second design framework, the structure of the introduced controllers is exploited to generate algorithms equipped with the back-calculation antiwindup term. It is noteworthy that linear and nonlinear designs are allowed by the two frameworks. The closed-loop stability is proved with the theory of singularly perturbed systems. To the best of the authors' knowledge, the use of theory of singularly perturbed systems in the study of saturated controls is new. With the aim of showing the validity of the stability theory as well as the accuracy of the proposed controllers, an experimental evaluation is presented.

This paper is organized as follows. Section II is devoted to the motor model and the velocity control objective. Section III concerns to the description and analysis of the proposed frameworks to design PI-like controllers. In Section IV, examples of the use of the proposed methodology are provided. The results of the experimental evaluation are given in Section V, while some concluding remarks are drawn in Section VI.

II. MODEL AND CONTROL GOAL

For the purpose of this paper, a motor with a drive having a voltage input u can be modeled by

$$J\ddot{q} + f_v\dot{q} = k \text{sat}(u) \quad (3)$$

where $\dot{q}(t)$ denotes the motor shaft velocity, $J > 0$ is the motor shaft inertia, $f_v > 0$ is the viscous friction coefficient, $k > 0$ is the so-called motor constant, and

$$\text{sat}(u) = \begin{cases} u^{\max}, & \text{for } u > u^{\max} \\ u, & \text{for } u^{\min} \leq u \leq u^{\max} \\ u^{\min}, & \text{for } u < u^{\min} \end{cases} \quad (4)$$

with $u^{\min} < 0$ the minimum voltage input and $u^{\max} > 0$ the maximum voltage input. The motor shaft velocity $\dot{q}(t)$ is measurable, thus the output of the system (3) is

$$y(t) = \dot{q}(t). \quad (5)$$

It is noteworthy that examples of motor drives that match the model (3)–(5) are the dc motors and induction motors operated by field-oriented control [2].

Control Problem: Consider the system (3), which involves the voltage saturation function (4). Assuming velocity measure-

ments $\dot{q}(t)$, the velocity control problem consists in designing a voltage control input $u(t)$ so that the velocity error

$$\dot{e}(t) = y^* - y(t) = \dot{q}_d - \dot{q}(t)$$

where \dot{q}_d is a constant that specifies the desired velocity, achieves the limit

$$\lim_{t \rightarrow \infty} \dot{e}(t) = \lim_{t \rightarrow \infty} [\dot{q}_d - \dot{q}(t)] = 0. \quad (6)$$

Solution proposed: As pointed out in Section I, many controllers have been proposed with the aim of solving the above-written regulation problem. However, most of these solutions consider the PI parts of the controller as linear functions.

In this paper, new solutions to the problem of velocity regulation input-saturated motors are provided. The main characteristics of the new algorithms are:

- 1) a PI structure is kept, which is familiar to control engineers;
- 2) nonlinear designs are allowed;
- 3) a backcalculation antiwindup loop can be added to a nonlinear PI design.

The closed-loop stability is proved rigorously. $\triangle\triangle\triangle$

III. TWO DESIGN FRAMEWORKS FOR SATURATED CONTROLLERS

In this section, two frameworks which allow designing linear and nonlinear controllers $u(t)$ for system (3) are introduced. Let us define the continuous and differentiable scalar functions $\phi_p(x)$ and $\phi_i(x)$ with properties

$$\phi_{p,i}(x)x > 0 \quad \forall x \in \mathbb{R}, \quad x \neq 0, \quad (7)$$

$$\phi_{p,i}(0) = 0 \quad (8)$$

$$\phi'_{p,i}(x) = \frac{\partial \phi_{p,i}(x)}{\partial x} > 0 \quad \forall x \in \mathbb{R}. \quad (9)$$

Subscripts p and i stand for PI, as these functions will be employed as components of a PI-like controller.

A. Framework I

A class of PI-like velocity regulators can be designed with the structure

$$u = \frac{1}{\epsilon} [\bar{k}_p \phi_p(\dot{e}) + \bar{k}_i \phi_i(\xi)] \quad (10)$$

$$\dot{\xi} = \dot{e} \quad (11)$$

where $\epsilon, \bar{k}_p, \bar{k}_i > 0$. The controller (10) and (11) can be implemented as

$$\frac{d}{dt} u = \frac{1}{\epsilon} [\bar{k}_p \phi'_p(\dot{e}) \ddot{e} + \bar{k}_i \phi'_i(\xi) \dot{\xi}]$$

with

$$u(0) = \frac{1}{\epsilon} [\bar{k}_p \phi'_p(\dot{e}(0)) \ddot{e}(0) + \bar{k}_i \phi'_i(\xi(0)) \dot{e}(0)].$$

Therefore, considering the solution $u(t)$ as the control input of the motor drive dynamics (3), the closed-loop system can be written in the form of a singularly perturbed system [12] as

$$\frac{d}{dt}\dot{e} = -\frac{f_v}{J}\dot{e} + \frac{f_v}{J}\dot{q}_d - \frac{k}{J}\text{sat}(u) \quad (12)$$

$$\epsilon \frac{d}{dt}u = \bar{k}_p \phi'_p(\dot{e})\ddot{e} + \bar{k}_i \phi'_i(\xi)\dot{e}. \quad (13)$$

For the sake of compactness, in the right-hand side of (13), we have decided to use the notation \ddot{e} , which can be replaced by (12).

Note that the closed-loop system (12) and (13) has an internal state $\xi(t) = \xi(0) + \int_0^t \dot{\xi}(x)dx$. Whereby we can consider it as a time-varying system (see [16] and [17] for a discussion on the analysis of interconnected nonlinear systems). In addition, as the exponential convergence of the signal $\dot{e}(t)$ is proven (see below), the signal $\xi(t)$ is uniformly bounded.

The closed-loop system (12) and (13) has a unique equilibrium point at

$$\begin{bmatrix} u \\ \dot{e} \end{bmatrix} = \begin{bmatrix} \frac{f_v \dot{q}_d}{k} \\ 0 \end{bmatrix}. \quad (14)$$

The existence and uniqueness of the equilibrium point is guaranteed with the assumption

$$u^{\min} \leq \frac{f_v \dot{q}_d}{k} \leq u^{\max}. \quad (15)$$

The system (12) and (13) has the form of a singularly perturbed system, where the gain ϵ is the perturbing parameter [12]. In general, a singularly perturbed system can be interpreted as a system composed by a slow dynamics subsystem and a fast dynamics subsystem.

To prove that the controller (10) and (11) guarantees velocity regulation of the input-saturated motor dynamics (3), we shall prove that there exists $\epsilon^* > 0$ such that the equilibrium point (14) of the closed-loop system (12) and (13) is locally exponentially stable with $\epsilon^* > \epsilon > 0$. This claim has been proven formally in [12, Th. 9.3], which, for the sake of completeness, is reproduced as Theorem 1 in Appendix A.

Proposition 1: There always exists $\epsilon^* > 0$ such that, for small enough $\epsilon^* > \epsilon > 0$, the equilibrium point (14) of the closed-loop system (12) and (13) is locally exponentially stable.

Proof: As pointed out before, Theorem 1 in Appendix A, which is related to the stability of singularly perturbed systems, will be invoked. The conditions required to apply such theorem are presented in an itemized form.

- 1) As previously shown, the system (12) and (13) has a unique equilibrium point given by $[u \ \dot{e}]^T = [f_v \dot{q}_d/k \ 0]^T \in \mathbb{R}^2$.
- 2) When $\epsilon = 0$, we obtain the quasi-steady-state equation

$$0 = \bar{k}_p \phi'_p(\dot{e})\ddot{e} + \bar{k}_i \phi'_i(\xi(t))\dot{e} \quad (16)$$

which has one isolated root

$$\begin{aligned} u &= \text{sat}^{-1}(h(\xi(t), \dot{e})) \\ &= h(\xi(t), \dot{e}) = \frac{c_2(\xi(t), \dot{e})}{c_1(\dot{e})} \end{aligned} \quad (17)$$

with

$$c_1 = \bar{k}_p \phi'_p(\dot{e}) \frac{k}{J} \quad (18)$$

$$c_2 = \bar{k}_p \phi'_p(\dot{e}) \frac{f_v}{J} \dot{q}_d + \left[\bar{k}_i \phi'_i(\xi(t)) - \bar{k}_p \phi'_p(\dot{e}) \frac{f_v}{J} \right] \dot{e}. \quad (19)$$

Equation (17) can always be satisfied with small enough fixed parameters $\xi(t), \dot{e} \in \mathbb{R}$. Besides, at $\dot{e} = 0$, the quasi-steady-state equation in (17) satisfies

$$u = h(\xi(t), 0) = f_v \dot{q}_d/k.$$

- 3) The right-hand side of (12) and (13) has bounded partial derivatives on compact sets.
- 4) With (12) and (16), the slow dynamics

$$\frac{d}{dt}\dot{e} = -\frac{\bar{k}_i}{k_p} \phi(t)\dot{e}$$

with $\phi(t) = \phi'_i(\xi(t))/\phi'_p(\dot{e})$, is obtained. Considering property (9), $\phi(t) > 0$ for all $t \geq 0$; hence, invoking the comparison lemma [12], the exponential convergence of $\dot{e}(t)$ can be proven.

- 5) The fast dynamics, i.e., the so-called boundary layer system [12], is obtained from (13) by defining the new time scale $\tau = t/\epsilon$, setting $\epsilon = 0$ and defining the new change of variable

$$y = u - h(\xi(t), \dot{e}) \quad (20)$$

with $h(\xi(t), \dot{e})$ in (17). Therefore, the boundary layer system is

$$\frac{d}{d\tau}y = -c_1 \text{sat}(y + h(\xi(t), \dot{e})) + c_2 \quad (21)$$

where c_1 and c_2 are given in (18) and (19), respectively, and $\xi(t), \dot{e} \in \mathbb{R}$ are interpreted as fixed parameters. Under assumption (17), the unique equilibrium point of the system (21) is $y = 0$.

It is worthwhile to note that, by using the change of variable (20), the boundary layer system can be rewritten as

$$\frac{d}{d\tau}u = -c_1 \text{sat}(u) + c_2 \quad (22)$$

whose unique equilibrium point is

$$u = h = c_2/c_1.$$

Because the convergence of $u(\tau) \rightarrow c_2/c_1$ as $\tau \rightarrow \infty$ implies $y(\tau) \rightarrow 0$ as $\tau \rightarrow \infty$, the forthcoming analysis will be based in analyzing the system (22). With this aim, let us define the positive definite function

$$W(u) = \frac{1}{2}[c_1 u - c_2]^2$$

whose time derivative is

$$\begin{aligned} \frac{d}{d\tau}W(u) &= -[c_1 u - c_2][c_1 \text{sat}(u) - c_2] \\ &\leq -[c_1 \text{sat}(u) - c_2]^2 \quad \forall u \in \mathbb{R}. \end{aligned} \quad (23)$$

The proof that inequality (23) holds is provided in Appendix B. Finally, the upper bound in (23), the change of variables (20), and the assumption (17) are used to claim that

$$\lim_{t \rightarrow \infty} \left[u(\tau) - \frac{c_2}{c_1} \right] = \lim_{t \rightarrow \infty} y(\tau) = 0$$

with exponential convergence rate.

By Theorem 1 in Appendix A, there are sufficient conditions to claim the existence of ϵ^* such that $\epsilon^* > \epsilon > 0$ guarantees the local exponential stability of the equilibrium point

$$\begin{bmatrix} u \\ \dot{e} \end{bmatrix} = \begin{bmatrix} \frac{f_v \dot{q}_d}{k} \\ 0 \end{bmatrix}$$

of the closed-loop system (12) and (13) for all initial conditions starting within the domain of attraction

$$R_A = \left\{ \begin{bmatrix} u \\ \dot{e} \end{bmatrix} \in \mathbb{R}^2 : \left\| \begin{bmatrix} u - \frac{f_v \dot{q}_d}{k} \\ \dot{e} \end{bmatrix} \right\| < d \right\}$$

that is

$$\begin{bmatrix} u(0) - \frac{f_v \dot{q}_d}{k} \\ \dot{e}(0) \end{bmatrix} \in R_A \Rightarrow \left\| \begin{bmatrix} u(t) - \frac{f_v \dot{q}_d}{k} \\ \dot{e}(t) \end{bmatrix} \right\| \leq k_1 e^{-k_2 t}$$

with some $k_1, k_2 > 0$. $\triangle\triangle\triangle$

Notice that the introduced stability analysis is simple, and the closed-loop exponential stability is guaranteed theoretically. However, in presence of noise, load disturbances and large integral gain, the performance of the controller (10) and (11) may present large settling time, overshoot, and potential instability. The addition of an antiwindup algorithm can be used to overcome these disadvantages. In the next section, we use this idea to propose a new class of controllers.

B. Framework II

A class of PI velocity regulators can be designed with the structure

$$u = [k_p \phi_p(\dot{e}) + k_i \phi_i(\xi)] - \frac{\bar{k}_{AW}}{\epsilon} \rho \quad (24)$$

$$\dot{\xi} = \dot{e} \quad (25)$$

$$\dot{\rho} = u - \text{sat}(u) \quad (26)$$

where $\epsilon, k_p, k_i, \bar{k}_{AW} > 0$.

To avoid windup, an extra feedback loop is added by feeding the integral of the difference between the controller output u and the saturated voltage input $\text{sat}(u)$ back to the controller output u times \bar{k}_{AW}/ϵ . If saturation occurs, the extra integral compensation brings the controller output u close to admissible values, and the performance of the unsaturated controller, i.e., $u = \text{sat}(u)$, is recovered faster. The rate at which the performance is recovered is governed by the term \bar{k}_{AW}/ϵ . An illustrative discussion of this fact is presented in [1]. Similarly

to the analysis shown in the previous section, the closed loop system is written as

$$\frac{d}{dt} \dot{e} = -\frac{f_v}{J} \dot{e} + \frac{f_v}{J} \dot{q}_d - \frac{k}{J} \text{sat}(u) \quad (27)$$

$$\epsilon \frac{d}{dt} u = \epsilon k_p \phi'_p(\dot{e}) \dot{e} + \epsilon k_i \phi'_i(\xi) \dot{\xi} - \bar{k}_{AW} [u - \text{sat}(u)]. \quad (28)$$

Due to the internal state $\xi(t)$, the system (27) and (28) can be considered as time varying [16], [17]. The properties on $\phi_p(\dot{e})$ and $\phi_i(\xi)$ and the theory of singularly perturbed systems guarantee that the closed-loop (27) and (28) is locally exponentially stable for small enough ϵ .

The equilibrium points of the closed-loop system (27) and (28) satisfy the equations

$$-\frac{f_v}{J} \dot{e} + \frac{f_v}{J} \dot{q}_d - \frac{k}{J} \text{sat}(u) = 0 \quad (29)$$

$$\epsilon k_i \phi'_i(\xi(t)) \dot{e} - \bar{k}_{AW} [u - \text{sat}(u)] = 0. \quad (30)$$

It is possible to show that the algebraic equation system (29) and (30) has only one solution

$$\begin{bmatrix} u \\ \dot{e} \end{bmatrix} = \begin{bmatrix} \frac{f_v \dot{q}_d}{k} \\ 0 \end{bmatrix} \quad (31)$$

where the assumption (15) is required.

Proposition 2: There always exists $\epsilon^* > 0$ such that for small enough $\epsilon^* > \epsilon > 0$, the equilibrium point (31) of the closed-loop system (27) and (28) is locally exponentially stable.

Proof: Similarly to the previous case, we apply Theorem 1 in Appendix A. The following conditions are required.

- 1) The system (27) and (28) has a unique equilibrium point, given by (31).
- 2) With $\epsilon = 0$, the *quasi-steady-state* solution is

$$u = \text{sat}(u). \quad (32)$$

Note that at the quasi-steady-state solution (32), the integration of (26) is

$$\rho(t) - \rho(0) = 0 \quad (33)$$

and, as $\rho(0)$ is an arbitrary initial condition, we can choose

$$\rho(0) = \epsilon \bar{\rho}(0) / \bar{k}_{AW}$$

so that the quasi-steady-state solution (32) can be written as

$$u = h(\xi(t), \dot{e}) = k_p \phi_p(\dot{e}) + k_i \phi_i(\xi(t)) - \bar{\rho}(0) \quad (34)$$

where $\xi(t)$ is obtained from (25).

It is noteworthy that by virtue of (32), the quasi-steady-state solution $h(\xi(t), \dot{e})$ in (34) satisfies

$$h(\xi(t), \dot{e}) = \text{sat}(h(\xi(t), \dot{e})). \quad (35)$$

Besides, at the equilibrium point (37), the quasi-steady-state equation (34) satisfies

$$u = h(\phi_i^{-1}(\gamma), 0) = f_v \dot{q}_d / k$$

which matches the equilibrium point (31) of the nonlinear system (27) and (28).

- 3) The right-hand side of (27) and (28) has bounded partial derivatives on compact sets.
- 4) By substituting (32) and (34) into (27), the slow dynamics

$$J\ddot{e} + f_v \dot{e} + k k_p \phi_p(\dot{e}) + k k_i \phi_i(\xi) - f_v \dot{q}_d - k \bar{\rho}(0) = 0 \tag{36}$$

is obtained, which is a second-order nonlinear system. The system (36) has a unique equilibrium point at

$$\begin{aligned} \begin{bmatrix} \xi \\ \dot{e} \end{bmatrix} &= \begin{bmatrix} \phi_i^{-1}(\gamma) \\ 0 \end{bmatrix} \\ \gamma &= \frac{f_v \dot{q}_d + k \bar{\rho}(0)}{k k_i}. \end{aligned} \tag{37}$$

Without loss of generality, we will assume that the inverse function $\phi_i^{-1}(\gamma)$ always exists.

A linear approximation of the slow dynamics (36) assures local exponential stability of the equilibrium point. Hence, $\dot{e}(t) \rightarrow 0$, with exponential convergence rate as time t increases. Furthermore, the global asymptotic stability of (36) can be proved with the Lyapunov function

$$V(\xi, \dot{e}) = \frac{J}{2} \dot{e}^2 + \int_0^\xi [k k_i \phi_i(x) - f_v \dot{q}_d - k \bar{\rho}(0)] dx + c$$

with some suitable constant c , and LaSalle's Theorem [12].

- 5) The boundary layer system is obtained from (28) by defining the new time scale $\tau = t/\epsilon$, setting $\epsilon = 0$, and defining the new change of variable

$$y = u - h(\xi(t), \dot{e}) \tag{38}$$

with $h(\xi(t), \dot{e})$ in (34) and $\xi(t), \dot{e} \in \mathbb{R}$ interpreted as fixed parameters. Thus, the boundary layer system is written as

$$\frac{d}{d\tau} y = -\bar{k}_{AW} [y + h(\xi(t), \dot{e}) - \text{sat}(y + h(\xi(t), \dot{e}))]. \tag{39}$$

Since the quasi-steady-state solution $h(\xi(t), \dot{e})$ satisfies (35), we conclude that the only equilibrium point of (39) is $y = 0$.

Consider the positive definite function

$$W(y) = \int_0^y [y + h - \text{sat}(y + h)] dy$$

whose time derivative is

$$\frac{d}{d\tau} W(y) = -\bar{k}_{AW} [y + h - \text{sat}(y + h)]^2. \tag{40}$$

On the other hand, it is possible to show that there are positive constants $\kappa_1, \kappa_2 > 0$ such that

$$\begin{aligned} \kappa_2 [y(\tau) + h - \text{sat}(y(\tau) + h)]^2 &\geq W(y) \\ &\geq \kappa_1 [y(\tau) + h - \text{sat}(y(\tau) + h)]^2 \end{aligned}$$

which make (40) satisfy

$$\frac{d}{d\tau} W(y) \leq -\frac{\bar{k}_{AW}}{\kappa_2} W(y).$$

Thus, the limit

$$\lim_{t \rightarrow \infty} [y(\tau) + h - \text{sat}(y(\tau) + h)] = 0 \tag{41}$$

is achieved with exponential convergence rate. Finally, invoking (35), the limit (41) implies that the limit

$$\lim_{t \rightarrow \infty} y(\tau) = 0 \tag{42}$$

is achieved exponentially.

Since all the conditions established in Theorem 1 in Appendix A are satisfied, there exists ϵ^* such that $\epsilon^* > \epsilon > 0$ guarantees that the equilibrium point

$$\begin{bmatrix} u \\ \dot{e} \end{bmatrix} = \begin{bmatrix} \frac{f_v \dot{q}_d}{k} \\ 0 \end{bmatrix}$$

is locally exponentially stable. △△△

In other words, in Proposition 2, we have proven that there is a compact set of initial conditions R_A , where the trajectories of the closed-loop system (27) and (28) achieve the limit

$$\lim_{t \rightarrow \infty} \begin{bmatrix} u(t) - \text{sat}(u(t)) \\ \dot{e}(t) \end{bmatrix} = 0. \tag{43}$$

Since the limit (43) is achieved exponentially, there is $T > 0$ such that, for all $t \geq T$

$$u(t) = \text{sat}(u(t))$$

which implies that the closed-loop system (27) and (28) can be rewritten as

$$\frac{d}{dt} \dot{e} = -\frac{f_v}{J} \dot{e} + \frac{f_v}{J} \dot{q}_d - \frac{k}{J} u \tag{44}$$

$$\epsilon \frac{d}{dt} u = \epsilon k_p \phi'_p(\dot{e}) \dot{e} + \epsilon k_i \phi'_i(\xi) \dot{e}. \tag{45}$$

That is, after a large enough time $t \geq T$, the closed-loop system (27) and (28) reduces to the system (44) and (45), which does not contain any saturation function. The system (44) and (45) is exponentially stable, and it can be interpreted as an unconstrained motor

$$J\ddot{q} + f_v \dot{q} = k u$$

controlled by the PI-like algorithms (10) and (11). Therefore, we can conclude that the limit (43) implies

$$\lim_{t \rightarrow \infty} \begin{bmatrix} u(t) \\ \dot{e}(t) \end{bmatrix} = \begin{bmatrix} \frac{f_v \dot{q}_d}{k} \\ 0 \end{bmatrix} \tag{46}$$

whereby the control objective (6) is satisfied with antiwindup-based controllers (24)–(26).

C. Implications in the Presence of an Embedded Current Loop

Many industrial motor drives are equipped with a servoamplifier that can operate in current mode, i.e., with a current control loop implemented inside the servoamplifier, which makes the motor’s input current equal to the desired current. If the control gains of the current loop are tuned with high gains, the electrical dynamics becomes less dominant than the mechanical one.

Now, we analyze in an informal way the implications of using either the class of controllers (10) and (11) or (24)–(26) in a motor drive that is connected to a servoamplifier operating in current mode. Let us consider the dynamics of an armature-controlled dc motor given by

$$J\ddot{q} + f_v\dot{q} = k_m i \tag{47}$$

$$L \frac{d}{dt} i + Ri = v - k_f \dot{q} \tag{48}$$

where $L, R, k_m, k_f > 0$, and v is the motor voltage input, which is provided by the servoamplifier usually containing a high-gain PI current controller, i.e.,

$$v(t) = k_p^* [k_{sa}\hat{u} - i(t)] + k_i^* \int_0^t [k_{sa}\hat{u} - i(t)] dt \tag{49}$$

where $k_{sa}\hat{u}$ is the desired current, k_{sa} the amplifier gain, $i(t)$ the actual current, k_p^* and k_i^* are the PI gains, respectively. Assuming that the current loop is implemented with high gains k_p^* and k_i^* , we can assume that the actual current $i(t)$ converges to the desired current $k_{sa}\hat{u}$ fast enough, so that

$$i(t) = k_{sa}\hat{u}. \tag{50}$$

In order to prevent excessive warming and a failure situation, the commanded current $k_{sa}\hat{u}$ should be limited by using

$$\hat{u} = sat(u)$$

where u corresponds to the output of the velocity loop, which may be defined either as the controller (10) and (11) or a scheme equipped with antiwindup (24)–(26).

Since practical current loops in motor drives are implemented with high gains, (50) is valid, and the motor model (47) and (48), operated with a servoamplifier using an embedded high-gain PI current loop, collapses into the model (3) with

$$k = k_m k_{sa}.$$

Therefore, a properly designed outer velocity loop, e.g., the class of controllers (10) and (11), renders the overall system exponentially stable.

IV. EXAMPLES

In this section, we show four design examples. The examples have the intention of showing how known and new controllers can be synthesized with the proposed frameworks.

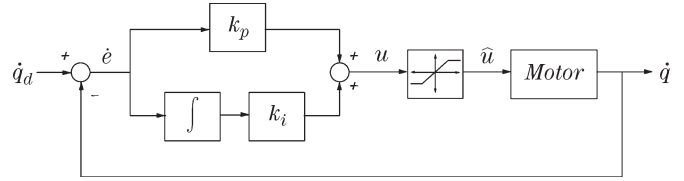


Fig. 1. Block diagram of the PI velocity control in cascade with a saturation function.

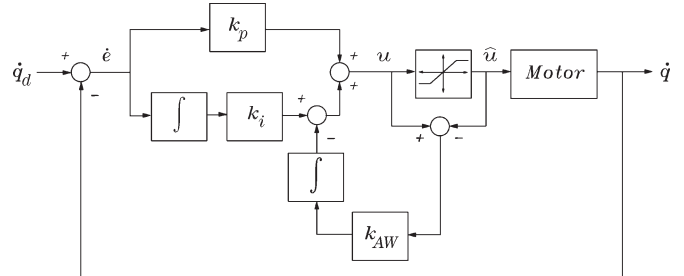


Fig. 2. Block diagram of the PI velocity controller equipped with the back-calculation antiwindup.

A. PI Control

The PI velocity controller is defined as [1], [5]

$$u = k_p \dot{e} + k_i \xi \tag{51}$$

$$\dot{\xi} = \dot{e} \tag{52}$$

where $k_p > 0$ and $k_i > 0$ are the PI gains of the controller, respectively.

The controller (51) and (52) is a particular case of the class of controllers (10) and (11), denoted as Design Framework I, with gains $k_p = \bar{k}_p/\epsilon$, $k_i = \bar{k}_i/\epsilon$, and functions $\phi_p(\dot{e}) = \dot{e}$, $\phi_p(\xi) = \xi$, clearly satisfying the properties (7)–(9).

To show the existence and uniqueness of the equilibrium point of the closed-loop system given by (3), (4), (51), and (52), the condition (15) should be satisfied.

Fig. 1 shows a block diagram of the PI controller (51) and (52), where

$$\hat{u} = sat(u) \tag{53}$$

is the effective control action, i.e., the voltage input that has effect on the motor dynamics.

B. PI Control Equipped With Antiwindup

Consider the PI velocity controller equipped with the back-calculation antiwindup [7] given by

$$u = k_p \dot{e} + k_i \xi - k_{AW} \rho \tag{54}$$

$$\dot{\xi} = \dot{e} \tag{55}$$

$$\dot{\rho} = u - \hat{u} \tag{56}$$

with $k_{AW} > 0$, and

$$\hat{u} = sat(u). \tag{57}$$

A block diagram of the controller (54)–(57) is shown in Fig. 2, being the saturation output \hat{u} , the effective control action applied to the motor.

With $k_{AW} = \bar{k}_{AW}/\epsilon$, the controller (54)–(56) belongs to the class of controllers (24)–(26) of the Design Framework II. Once again, $\phi_p(\dot{e}) = \dot{e}$ and $\phi_p(\xi) = \xi$, satisfying the properties required in (7)–(9).

Under assumption (15), the only equilibrium point of the closed-loop system is given by

$$\begin{bmatrix} u \\ \dot{e} \end{bmatrix} = \begin{bmatrix} \frac{f_v \dot{q}_d}{k} \\ 0 \end{bmatrix}.$$

It is worthwhile noticing that the controller (54)–(56) can be implemented as

$$u = k_p \dot{e} + k_i \xi \tag{58}$$

$$\dot{\xi} = \dot{e} - \frac{k_{AW}}{k_i} [u - \text{sat}(u)] \tag{59}$$

that is, using only one integrator.

C. satPI Control

A new velocity controller is introduced as follows:

$$u = k_p \sigma(\lambda_p \dot{e}) + k_i \sigma(\lambda_i \xi) \tag{60}$$

$$\dot{\xi} = \dot{e} = \dot{q}_d - \dot{q} \tag{61}$$

where k_p , k_i , λ_p , and λ_i are strictly positive constants, and the saturation function $\sigma(\cdot)$ is defined in [21] as

$$\sigma(\lambda_{p,i} x) = \begin{cases} -l + [m - l] \tanh\left(\frac{\lambda_{p,i} x + l}{m - l}\right), & \text{if } \lambda_{p,i} x < -l \\ \lambda_{p,i} x, & \text{if } |\lambda_{p,i} x| \leq l \\ l + [m - l] \tanh\left(\frac{\lambda_{p,i} x - l}{m - l}\right), & \text{if } \lambda_{p,i} x > l \end{cases} \tag{62}$$

where $l > 0$, $m > 0$, $m \neq l$, and subindexes p and i refer to the PI parts of the controller (60), respectively.

The PI parts of the controller (60) and (61) are nonlinear functions. A reason to use the saturation function (62) in this new design is that it incorporates the extra parameters λ_p , λ_i , l , and m , whose numerical values have the effect of changing the slope of the profile of the saturation function. Therefore, we can either reinforce or attenuate the contribution of each part of the controller by selecting the parameters involved in the saturation function (62). See Fig. 3 for examples of the saturation function (62) presenting different profiles.

As in the previously described schemes, the only equilibrium point of the closed-loop system generated by the motor drive model (3) and controller (60) and (61) is given by

$$\begin{bmatrix} u \\ \dot{e} \end{bmatrix} = \begin{bmatrix} \frac{f_v \dot{q}_d}{k} \\ 0 \end{bmatrix}.$$

Fig. 4 shows a block diagram of the implementation of the controller (60) and (61).

The controller introduced in (60) and (61) belongs to the class of controllers (10) and (11) of Design Framework I with $k_p = \bar{k}_p/\epsilon$, $k_i = \bar{k}_i/\epsilon$, $\phi_{p,i}(x) = \sigma(\lambda_{p,i} x)$, $x \in \mathbb{R}$, and the sub-

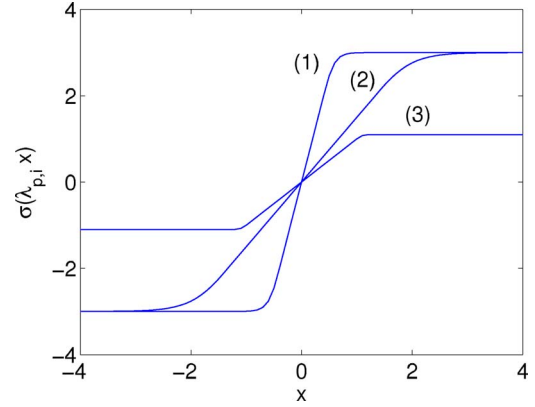


Fig. 3. Examples of profiles of the saturation function $\sigma(\lambda_{p,i} x)$ in (62). (1) $(\lambda_{p,i}, l, m) = (5, 2, 3)$. (2) $(\lambda_{p,i}, l, m) = (1.5, 2, 3)$. (3) $(\lambda_{p,i}, l, m) = (1, 1, 1.1)$.

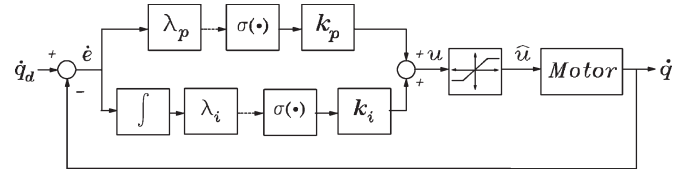


Fig. 4. Block diagram of the new saturated PI velocity controller.

script p and i refers to the PI parts of the controller, respectively. The property (7) is satisfied because

$$\phi_{p,i}(x)x = \sigma(\lambda_{p,i} x)x > 0 \quad \forall x \in \mathbb{R}, \quad x \neq 0.$$

Besides, $\sigma(0) = 0$, whereby property (8) is fulfilled. Finally, property (9) is verified as follows:

$$\begin{aligned} \frac{\partial \phi_{p,i}(x)}{\partial x} &= \frac{\partial \sigma(\lambda_{p,i} x)}{\partial x} \\ &= \begin{cases} \lambda_{p,i} \text{sech}^2\left(\frac{\lambda_{p,i} x + l}{m - l}\right), & \text{if } \lambda_{p,i} x < -l \\ \lambda_{p,i}, & \text{if } |\lambda_{p,i} x| \leq l \\ \lambda_{p,i} \text{sech}^2\left(\frac{\lambda_{p,i} x - l}{m - l}\right), & \text{if } \lambda_{p,i} x > l \end{cases} \end{aligned}$$

which is a strictly positive function for all $x \in \mathbb{R}$.

D. satPI + AW Control

An antiwindup loop can be added to the control law (60) and (61) as follows:

$$u = k_p \sigma(\lambda_p \dot{e}) + k_i \sigma(\lambda_i \xi) - k_{AW} \rho \tag{63}$$

$$\dot{\xi} = \dot{e} = \dot{q}_d - \dot{q} \tag{64}$$

$$\dot{\rho} = u - \hat{u} \tag{65}$$

where k_p , k_i , λ_p , λ_i , and k_{AW} are strictly positive constants, and $\hat{u} = \text{sat}(u)$. The controller (63)–(65) corresponds to the class of controllers described as Design Framework II in Section III-B.

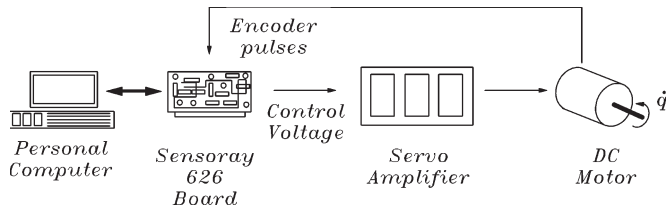


Fig. 5. Block diagram of the experimental system.

V. EXPERIMENTAL RESULTS

In order to evaluate the performance of the studied controllers, we have carried out real-time experiments on a *Pittman 14207S008* dc motor driven by a servoamplifier model *30A20AC* from *Advanced Motion Controls*, which is configured in current mode. To execute real-time experiments the motor is controlled through a PC and a data acquisition board *Sensoray 626*, which is used to read the quadrature optical encoder signals and transfer the control signal to the servoamplifier. Fig. 5 shows a block diagram of the experimental system. Algorithms are executed at a sampling frequency of 1 kHz on *Windows XP* using *Matlab* with *Simulink* and the *Real-Time Windows Target*.

The aim of the experimental evaluation is to show that, by using controllers derived from the two frameworks introduced in Section III, a good performance in the velocity regulation and disturbance rejection can be obtained, in comparison to known approaches.

Some important details of our experimental set-up are provided as follows. The pulsewidth-modulation (PWM) servoamplifier is designed to drive brush-type dc motors at a high switching frequency. The servoamplifier is operated in current mode with

$$k_{sa} = 1.36 \text{ A/V}.$$

Neglecting the power limitation, the system composed by the servoamplifier and the dc motor can be modeled in the Laplace domain as

$$G(s) = \frac{\dot{q}(s)}{u(s)} = \frac{k/J}{s + f_v/J} \frac{\text{rad}}{\text{V} \cdot \text{s}}. \quad (66)$$

By using the least-squares parameter identification method, we computed the following transfer function parameters:

$$\frac{k}{J} = 1000.0 \text{ [rad/(V} \cdot \text{s}^2\text{)]} \quad \frac{f_v}{J} = 1.9 \text{ 1/s}. \quad (67)$$

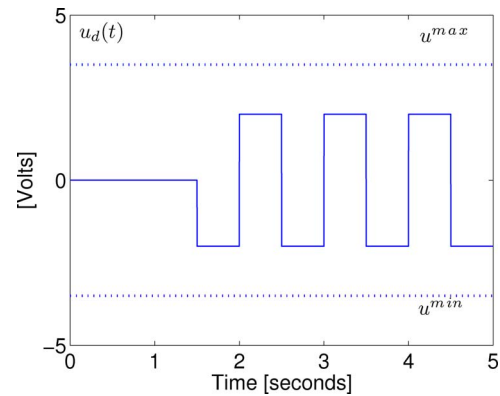
The specifications of the motor manufacturer indicate that the maximum continuous torque is obtained at

$$|i^{\max}| = 5 \text{ A}.$$

Therefore, the maximum applied voltage is

$$|u^{\max}| = |i^{\max}|/k_{sa} = 3.68 \text{ V}.$$

As a simple protection criterion that can be used in applications where the current is less than 5 A, respectively 3.68 V, let us


 Fig. 6. Time evolution of the voltage disturbance $u_d(t)$.

use the following symmetric voltage constraints:

$$\begin{aligned} u^{\max} &= 3.5 \text{ V} \\ u^{\min} &= -3.5 \text{ V}. \end{aligned} \quad (68)$$

In the experiments, the desired velocity was

$$\dot{q}_d = 250 \text{ rad/s} = 2387.32 \text{ rev/min}. \quad (69)$$

At this speed, the motor dissipates 180 W, i.e., 80% of the maximum power specified by the manufacturer.

In order to test the performance of the controllers evaluated experimentally, a square-wave voltage disturbance $u_d(t)$ which has 2 V of amplitude was added to the motor voltage input, i.e.,

$$J\ddot{q} + f_v\dot{q} = k[\text{sat}(u) + u_d].$$

Let us notice that the signal $u_d(t)$ models load disturbances. See Fig. 6 to see the evolution of the voltage disturbance $u_d(t)$.

Because of the specified velocity \dot{q}_d , the voltage constraints (68), and the voltage disturbance $u_d(t)$, we can consider that our experimental setup matches an industrial scenery.

A. PI Control

The first experiment consists in implementing the PI controller (51) and (52) by using the velocity reference (69), and the saturation limits (68).

The control gains were selected as follows. Neglecting the saturation function and considering the motor model under PI control (51) and (52), the closed-loop transfer function can be written as

$$\frac{\dot{q}(s)}{\dot{q}_d(s)} = \frac{\frac{k}{J}k_p s + \frac{k}{J}k_i}{s^2 + \left[\frac{f_v}{J} + \frac{k}{J}k_p\right]s + k_i \frac{k}{J}}. \quad (70)$$

By using the relationship

$$k_p = \frac{2\sqrt{\frac{k}{J}k_i} - \frac{f_v}{J}}{\frac{k}{J}} \quad (71)$$

the poles of the transfer function (70) are repeated.

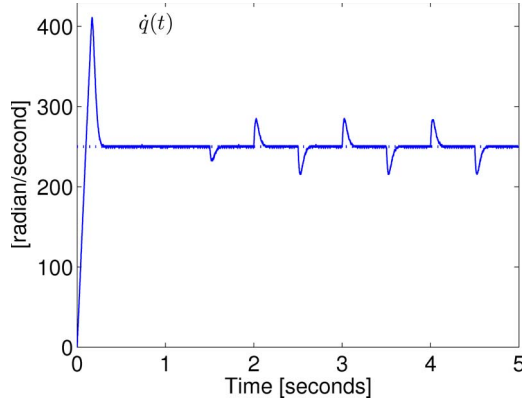


Fig. 7. PI control: velocity $\dot{q}(t)$.

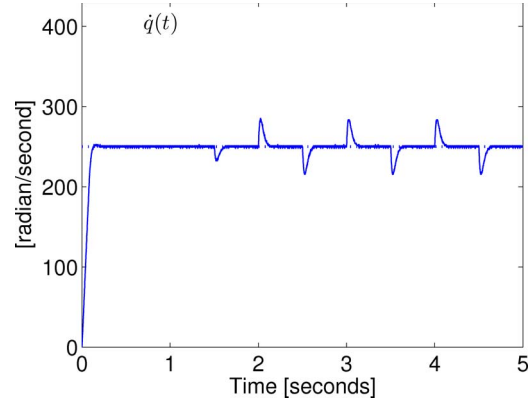


Fig. 9. PI control + AW: velocity $\dot{q}(t)$.

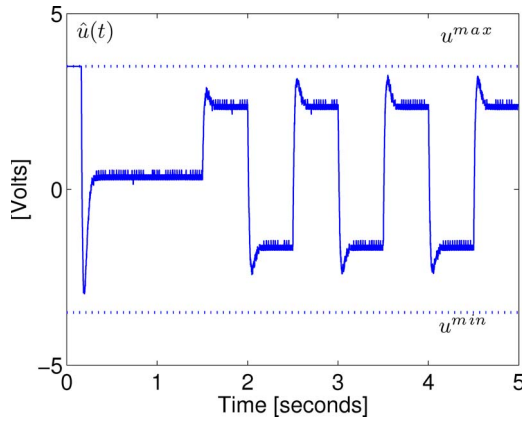


Fig. 8. PI control: effective control action $\hat{u}(t)$.

By substituting the gains

$$\begin{aligned} k_p &= 0.0875 \text{ V} \cdot \text{s/rad} \\ k_i &= 2 \text{ V/rad} \end{aligned} \quad (72)$$

which satisfy (71), and the numerical values of the motor parameters (67) into the transfer function (70), we have

$$\frac{\dot{q}(s)}{\dot{q}_d(s)} = \frac{87.5s + 2000.0}{s^2 + 89.4s + 2000.0}$$

which has poles located at

$$s_{1,2} = -44.72.$$

The theoretical percent overshoot is 12%, and the rise time $t_s = 0.064 \text{ s}$.

The PI controller in (51)–(53) has been implemented with the gains (72). The time history of the velocity response $\dot{q}(t)$ is shown in Fig. 7, while the effective control action $\hat{u}(t)$ is shown in Fig. 8.

As shown in Fig. 7, a large overshoot in the velocity response $\dot{q}(t)$ is obtained. This resulted because of the saturation of the control action $\hat{u}(t)$ and the numerical accumulation of the integrator $\xi(t)$.

B. PI Control + Antiwindup

In order to make a fair comparison with respect to the PI controller (51)–(53), we have implemented the PI controller

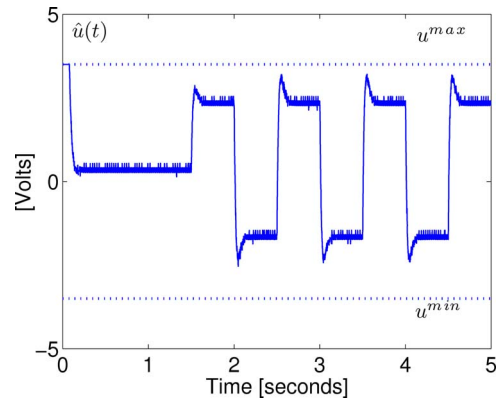


Fig. 10. PI control + AW: effective control action $\hat{u}(t)$.

plus antiwindup (58) and (59) using the saturation limits (68), the desired velocity \dot{q}_d in (69), the control gains k_p , k_i in (72), and

$$k_{AW} = 50 \text{ 1/s} \quad (73)$$

which was selected by trial and error until the best performance was obtained. Let us notice that in [1], the tuning rule

$$\frac{k_p}{k_i} > \frac{1}{k_{AW}}$$

is suggested, which is accomplished by the gains in (72) and (73).

The results are given in Figs. 9 and 10, which show the velocity $\dot{q}(t)$ and the effective control action $\hat{u}(t)$, respectively. Note that a nice response is observed for the velocity $\dot{q}(t)$ which converges rapidly to the desired value \dot{q}_d , while $\hat{u}(t)$ remains saturated during a short time.

C. satPII Control

We have denoted as *satPII* the implementation of the controller (60) and (61) using the saturation function (62) with $\lambda_{p,i} = 1$, $l = 25$, $m = 26$, the desired velocity \dot{q}_d in (69), k_p and k_i in (72), and the saturation limits in (68).

Fig. 11 shows the time history of the velocity $\dot{q}(t)$ and Fig. 12 shows the effective control action $\hat{u}(t)$. Some transients are observed, but after a short time, the velocity $\dot{q}(t)$ reaches the desired value \dot{q}_d .

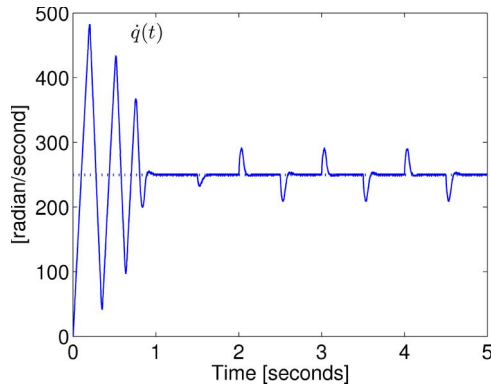


Fig. 11. satPI1 control: velocity $\dot{q}(t)$.

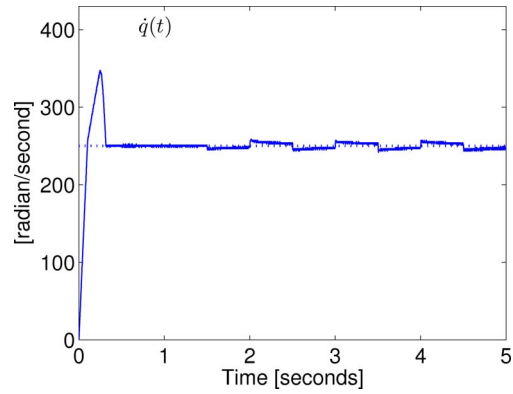


Fig. 13. satPI2 control: velocity $\dot{q}(t)$.

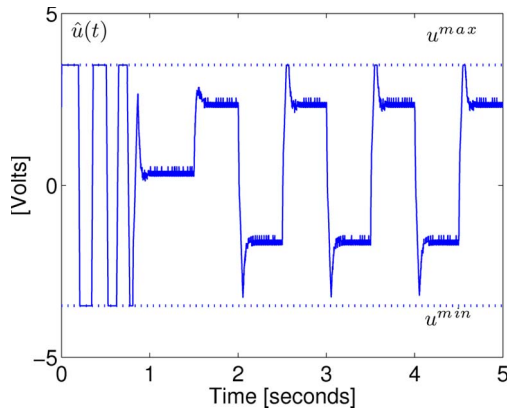


Fig. 12. satPI1 control: effective control action $\hat{u}(t)$.

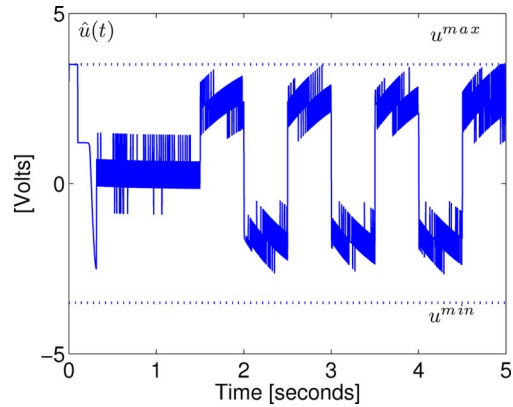


Fig. 14. satPI2 control: effective control action $\hat{u}(t)$.

D. satPI2 Control

One important observation is that the performance of the previous case *satPI1* was not so good as the one obtained with the PI + AW controller (58) and (59). The explanation is that the new controller (60) and (61) incorporates the nonlinear function (62) to compute the PI parts of the controller.

Simulations and previous experiments showed that the performance of the new controller is strongly related to the gains k_p and k_i , as well as the parameters $(\lambda_{p,i}, l, m)$. In order to show this, a second experiment with the new controller (60) and (61) was carried out using the control gains

$$k_p = 0.5 \text{ V} \cdot \text{s/rad}$$

$$k_i = 0.7 \text{ V/rad}$$

and the parameters $\lambda_{p,i} = 1, l = 5$, and $m = 6$ in the saturation function (62). We will denote this design example as *satPI2*. The results of this experiment are in Fig. 13, where the time history of the velocity $\dot{q}(t)$ is exhibited, and in Fig. 14, which shows the effective control action $\hat{u}(t)$. Overshoot is present in the velocity response. However, once in steady state, the controller is able to reject the voltage disturbances since the actual velocity $\dot{q}(t)$ presents small deviations from the desired velocity \dot{q}_d .

E. Discussions

In the four experiments, the velocity response $\dot{q}(t)$ tends to the desired velocity \dot{q}_d in a relatively short time, but different transients were observed.

TABLE I
PERFORMANCE OF THE FOUR CONTROLLERS

Index	PI	PI+AW	satPI1	satPI2
Percent overshoot	64%	0%	92.8%	38.4%
Settling time [sec]	0.238	0.093	0.87	0.307
$E = \int_0^5 \hat{u}(t)^2 dt$	18.556	17.349	25.573	17.918
$ \dot{e} _P$	35.1	35.1	41.4	8.5

The percent overshoot and settling time have been computed for each of the four experiments (see Table I). With respect to these indexes, the classical controller PI + antiwindup (58) and (59) presented the best performance.

For all the controllers evaluated experimentally, the effective control action $\hat{u}(t) = sat(u(t))$ has an oscillatory and noisy behavior. To see these effects, compare Figs. 8, 10, 12, and 14. We have computed an energylike index of the effective control action $\hat{u}(t)$, i.e.,

$$E = \int_0^5 \hat{u}(t)^2 dt.$$

The results are given in Table I, and in Fig. 15, which shows a bar chart of E . With respect to this index, the best performance is obtained for the PI + antiwindup (58) and (59) controller. However, the index E for the *satPI2* controller (60) and (61) is very similar to the one for the PI + antiwindup, just 3.28% higher.

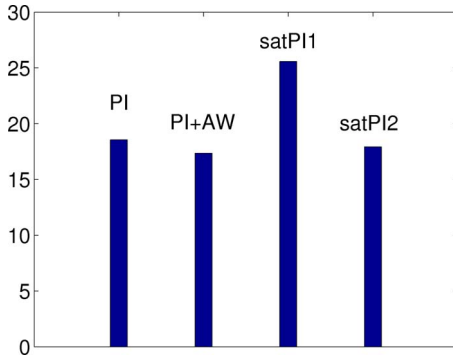


Fig. 15. Bar chart of $E = \int_0^5 \dot{u}(t)^2 dt$ computed for the four controllers evaluated experimentally.

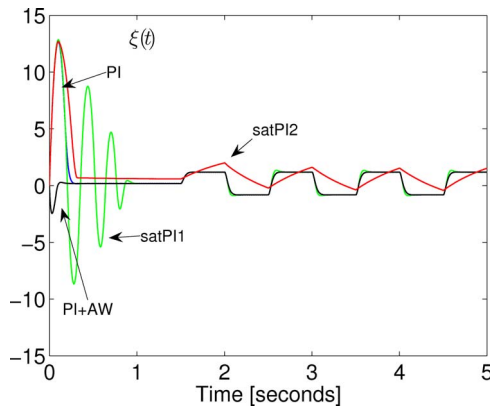


Fig. 16. Time evolution of the integral variable $\xi(t)$ for the four controllers evaluated experimentally.

On the other hand, note that voltage disturbances $u_d(t)$ are present after 1.5 [s]. A useful index to measure the ability of the controllers to reject the voltage disturbances is the velocity error peak, which is defined as

$$|\dot{e}|_P = \max_{\forall t \geq 1.5} \{|\dot{e}(t)|\}.$$

Table I summarizes the information about the velocity error peak $|\dot{e}|_P$. The best performance was obtained for the new controller in the design example *satPI2*.

Due to discretization, quantization errors, and high-frequency PWM switching of the servoamplifier, high-frequency components appear in the control signal. These components can be either increased or decreased with the control gains; in particular, we noticed that they were affected by the value of the proportional gain. However, in spite of the high-frequency contents in the voltage control signal, we did not observe negative effects in the performance of the motor, such as mechanical vibrations.

Finally, the value of the integral variable can be used as a measure of the “degree of windup” in the closed-loop system. The value of the integral of the velocity error $\xi(t) = \int_0^t \dot{e}(x) dx$ for each controller implemented is shown in Fig. 16.

It is noteworthy that for the PI + AW controller (58) and (59), the signal $\xi(t)$ is rapidly attenuated because $\xi(t)$ is recomputed when the controller is saturated. The variation of $\xi(t)$ after 1.5 [s] is due to the presence of the voltage disturbance $u_d(t)$.

In the case of the *satPI2* controller (60) and (61), using the control gains given in Section V-D, it is noticeable that the signal $\xi(t)$ decreases more slowly than in the case of the PI + AW controller (58) and (59).

The experimental evidence showed that in the new design *satPI2*, the behavior of $\xi(t)$ is enough to reject the voltage disturbances $u_d(t)$.

VI. CONCLUSION

In this paper, a large class of velocity regulators for input-saturated motor drives has been introduced. On the basis of the previous theory and experiments, the main conclusions of this paper are as follows.

- 1) The use of the stability theory of singularly perturbed systems showed how controllers can be easily synthesized while local exponential stability is guaranteed.
- 2) Two controllers previously proposed in the literature belong to this class of regulators, while a new one was introduced.
- 3) The experimental results showed that saturated nonlinear PI control can be efficient to regulate the motor shaft velocity. In particular, the rejection to disturbances was better in the implementation of the design example *satPI2* than in the implementation of the known approaches.

APPENDIX A

A singularly perturbed system can be decoupled in two subsystems: A slow dynamics subsystem and a fast dynamics subsystem. Under certain conditions, the exponential stability of each subsystem implies that the overall system is exponentially stable. This claim has been stated formally in [12, Th. 9.3], which is reproduced below as Theorem 1. The symbol B_r denotes the set given by the ball $\{\mathbf{x} \in \mathbb{R}^n : \|\mathbf{x}\| \leq r\}$.

Theorem 1: Consider the singularly perturbed system

$$\dot{\mathbf{x}} = \mathbf{f}(t, \mathbf{x}, \mathbf{z}, \epsilon), \quad \mathbf{x} \in \mathbb{R}^{n_1} \quad (74)$$

$$\epsilon \dot{\mathbf{z}} = \mathbf{g}(t, \mathbf{x}, \mathbf{z}, \epsilon), \quad \mathbf{z} \in \mathbb{R}^{n_2} \quad (75)$$

and $\epsilon > 0$. Assume that the following assumptions are satisfied for all:

$$(t, \mathbf{x}, \epsilon) \in [0, \infty) \times B_r \times [0, \epsilon_0].$$

- 1) $\mathbf{f}(t, \mathbf{0}, \mathbf{0}, \epsilon) = \mathbf{0}$ and $\mathbf{g}(t, \mathbf{0}, \mathbf{0}, \epsilon) = \mathbf{0}$.
- 2) The equation

$$\mathbf{0} = \mathbf{g}(t, \mathbf{x}, \mathbf{z}, 0)$$

has an isolated root $\mathbf{z} = \mathbf{h}(t, \mathbf{x})$ such that $\mathbf{h}(t, \mathbf{0}) = \mathbf{0}$.

- 3) The functions \mathbf{f} , \mathbf{g} , and \mathbf{h} and their partial derivatives up to order 2 are bounded for $\mathbf{z} - \mathbf{h}(t, \mathbf{x}) \in B_\rho$.

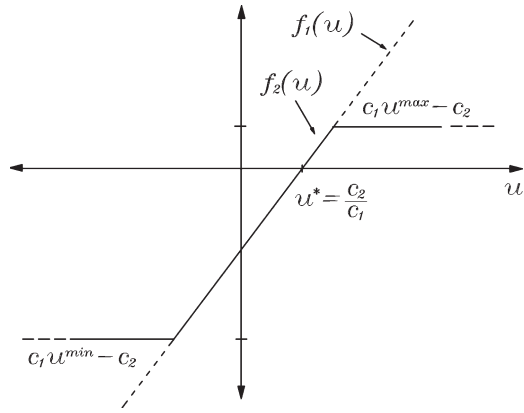


Fig. 17. Graph of $f_1(u)$ and $f_2(u)$ assuming $c_2 > 0$.

4) The origin of the reduced system

$$\dot{\mathbf{x}} = \mathbf{f}(t, \mathbf{x}, \mathbf{h}(t, \mathbf{x}), 0) \tag{76}$$

is exponentially stable.

5) The origin of the boundary-layer system

$$\frac{d\mathbf{y}}{d\tau} = \mathbf{g}(t, \mathbf{x}, \mathbf{y} + \mathbf{h}(t, \mathbf{x}), 0) \tag{77}$$

$\tau = t/\epsilon$, $\mathbf{y} = \mathbf{z} - \mathbf{h}(t, \mathbf{x})$, is exponentially stable, uniformly in (t, \mathbf{x})

Then, there exists $\epsilon^* > 0$ such that, for all $\epsilon < \epsilon^*$, the origin of (74) and (75) is exponentially stable.

Proof: See [12, p. 380]. △△△

APPENDIX B

Let us discuss an important property of the saturation function (4). Consider two constants $c_1 > 0$, $c_2 \in \mathbb{R}$, and the functions

$$f_1(u) = c_1 u - c_2 \tag{78}$$

$$f_2(u) = c_1 \text{sat}(u) - c_2. \tag{79}$$

In order to guarantee that $f_2(u)$ crosses the u axis, the following assumption is required:

$$u^{\min} \leq \frac{c_2}{c_1} \leq u^{\max}. \tag{80}$$

Hence,

$$f_2(u^*) = 0, \quad \text{with } u^* = \frac{c_2}{c_1}.$$

A graphical description of $f_1(u)$ and $f_2(u)$ in (78) and (79), satisfying assumption (80), is shown in Fig. 17.

Let us suppose that $u \leq u^*$, then

$$f_1(u) \leq f_2(u) \leq 0.$$

Multiplying by $f_2(u)$

$$f_1(u)f_2(u) \geq f_2(u)^2 \geq 0.$$

Now, suppose that $u \geq u^*$, then

$$f_1(u) \geq f_2(u) \geq 0.$$

Similarly, multiplying by $f_2(u)$

$$f_1(u)f_2(u) \geq f_2(u)^2 \geq 0.$$

Therefore, we have shown that

$$f_1(u)f_2(u) \geq f_2(u)^2 \geq 0 \quad \forall u \in \mathbb{R}.$$

REFERENCES

- [1] K. Åström and T. Häggglund, *PID Controllers: Theory, Design, and Tuning*, 2nd ed. Research Triangle Park, NC: ISA, 1995.
- [2] I. Boldea and S. A. Nasar, *Vector Control of AC Drives*. Boca Raton, FL: CRC Press, 1992.
- [3] P. I. Corke, "The unimation PUMA servo system," Division Manuf. Technol., CSIRO, Preston, Australia, Tech. Rep. MTM-226, 1994.
- [4] K. E. Daggett, E. M. Onaga, and R. J. Casler, Jr., "Position and velocity feedback system for a digital robot control," U.S. Patent 4876 494, Oct. 24, 1989.
- [5] R. Dorf and R. Bishop, *Modern Control Systems*, 10th ed. Upper Saddle River, NJ: Prentice-Hall, 2004.
- [6] Y. Eun, P. T. Kabamba, and S. M. Meerkov, "System types in feedback control with saturating actuators," *IEEE Trans. Autom. Control*, vol. 49, no. 2, pp. 287–291, Feb. 2004.
- [7] H. A. Fertik and C. W. Ross, "Direct digital control algorithms with anti-windup feature," *ISA Trans.*, vol. 6, no. 4, pp. 317–328, 1967.
- [8] P. Kapasouris, M. Athans, and G. Stein, "Design of feedback control systems for stable plants with saturating actuators," in *Proc. 27th IEEE Conf. Decision Control*, Austin, TX, Dec. 7–9, 1988, pp. 469–479.
- [9] A. S. Hodel and E. C. E. Hall, "Variable-structure PID control to prevent integrator windup," *IEEE Trans. Ind. Electron.*, vol. 45, no. 3, pp. 445–450, Jun. 1998.
- [10] F. Jatta, G. Legnani, and A. Visioli, "Friction compensation in hybrid force/velocity control of industrial manipulators," *IEEE Trans. Ind. Electron.*, vol. 53, no. 2, pp. 604–613, Apr. 2006.
- [11] C. Jo, J. Y. Seol, and I. J. Ha, "Flux-weakening control of IPM motors with significant effect of magnetic saturation and stator resistance," *IEEE Trans. Ind. Electron.*, vol. 55, no. 3, pp. 1330–1340, Mar. 2008.
- [12] H. Khalil, *Nonlinear Systems*. Upper Saddle River, NJ: Prentice-Hall, 1996.
- [13] M. V. Khotare, P. J. Campo, M. Morari, and C. N. Nett, "A unified framework for the study of anti-windup designs," *Automatica*, vol. 30, no. 12, pp. 1869–1883, Dec. 1994.
- [14] R. J. Mantz and H. De Battista, "Comments on 'variable-structure PID control to prevent integrator windup'," *IEEE Trans. Ind. Electron.*, vol. 51, no. 3, pp. 736–738, Jun. 2004.
- [15] J. Moreno and R. Kelly, "On motor velocity control by using only position measurements: Two case studies," *Int. J. Elect. Eng. Educ.*, vol. 39, no. 2, pp. 118–127, 2002.
- [16] E. Panteley and A. Loria, "On global uniform asymptotic stability of nonlinear time-varying systems in cascade," *Syst. Control Lett.*, vol. 33, no. 2, pp. 131–138, Feb. 1998.
- [17] E. Panteley and A. Loria, "Growth rate conditions for stability of cascaded time-varying systems," *Automatica*, vol. 37, no. 3, pp. 453–460, Mar. 2001.
- [18] J. K. Seok, K. T. Kim, and D. C. Lee, "Automatic mode switching of P/PI speed control for industry servo drives using online spectrum analysis of torque command," *IEEE Trans. Ind. Electron.*, vol. 54, no. 5, pp. 2642–2647, Oct. 2007.
- [19] J.-J. E. Slotine and W. Li, *Applied Nonlinear Control*. Englewood Cliffs, NJ: Prentice-Hall, 1991.
- [20] H. B. Shin, "New antiwindup PI controller for variable-speed motor drives," *IEEE Trans. Ind. Electron.*, vol. 45, no. 3, pp. 445–450, Jun. 1998.
- [21] A. Zavala-Rio and V. Santibáñez, "A natural saturating extension of the PD-with-gravity-compensation control law for robot manipulators with bounded inputs," *IEEE Trans. Robot.*, vol. 23, no. 2, pp. 386–391, Apr. 2007.



Javier Moreno-Valenzuela was born in Culiacán, Mexico, in 1974. He received the Ph.D. degree in automatic control from the Centro de Investigación Científica y de Educación Superior de Ensenada, Ensenada, Mexico, in 2002.

From 2004 to 2005, he was a Postdoctoral Fellow with the Université de Liège, Belgium. He is currently with the Centro de Investigación y Desarrollo de Tecnología Digital del Instituto Politécnico Nacional, Tijuana, Mexico. His main research interests are control of electromechanical systems, robotics,

and real-time systems.



Ricardo Campa (M'97) was born in Torreón, Mexico, in 1971. He received the M.S. degree in electrical engineering from the Instituto Tecnológico de la Laguna, Torreón, in 1998, and the Ph.D. degree in electronics and telecommunications from Centro de Investigación Científica y de Educación Superior de Ensenada, Ensenada, Mexico, in 2005.

He is currently a Research Professor with the División de Estudios de Posgrado e Investigación, Instituto Tecnológico de la Laguna. His research interests include modeling and control of robotic

systems, pose control, path planning, and real-time applications.